New view of the occupied band structure of Mo(112)

Keisuke Fukutani,[1] Hirokazu Hayashi,[2] Ivan N. Yakovkin,[3] Tula R. Paudel,[1] Takafumi Habuchi,[2] Daisuke Hirayama,[2] Jian Jiang,[2] Hideaki Iwasawa,[2] Kenya Shimada,[2] Ning Wu,[1] Evgeny Y. Tsymbal,[1] Ya. B. Losovyj,[4] and P. A. Dowben[1,*]

[1]*Department of Physics and Astronomy, Jorgensen Hall, P.O. Box 880299, University of Nebraska-Lincoln, Lincoln, Nebraska 68588-0299, USA*

[2]*Hiroshima Synchrotron Radiation Center, Hiroshima University, 2313 Kagamiyama, Higashi-Hiroshima, Hiroshima 7390046, Japan*

[3]*Institute of Physics, National Academy of Sciences of Ukraine, Prospect Nauki 46, Kiev, UA 03039, Ukraine*

[4]*The J. Bennett Johnston Sr. Center for Advanced Microstructures and Devices, Louisiana State University, 6980 Jefferson Hwy., Baton Rouge, Louisiana 70806, USA*

(Received 30 December 2011; published 19 April 2012)

We present a comprehensive examination of the occupied surface-weighted band structure of Mo(112) along the two high-symmetry directions of the surface Brillouin zone, both from theoretical and experimental perspectives. The band structures are found to be significantly different for the states along the two high-symmetry directions and for the states with even and odd reflection parities with respect to the mirror planes. The present study suggests the existence of a number of surface-weighted bands along both high-symmetry directions. The complexity of the band structure near the Fermi level may impose potential difficulties in experimental determination of the electron-phonon coupling parameters based on the effective mass enhancement distortion (or kink) in the energy-band dispersion, in the vicinity of the Fermi level, for several surface resonance bands of Mo(112).

DOI: 10.1103/PhysRevB.85.155435 PACS number(s): 73.20.At, 63.20.kd, 73.61.At

I. INTRODUCTION

The surfaces of molybdenum are among the most studied in surface science, yet the detailed picture of their electronic structures as well as their many-body interactions remains incomplete. Surface states and surface resonance states in solids have a very long history,[1–6] and the existence of surface resonance states was first verified for Mo(100) in 1977[7,8] and subsequently characterized in more detail both theoretically and experimentally.[9] More recently, high-resolution angle-resolved photoemission spectroscopy (ARPES) made it possible to extract the detailed surface band structures of solids, which led to the elucidation of many-body interactions and their effects on the electronic structures of molybdenum surfaces.[10,11] In particular, theoretically predicted small yet characteristic band renormalization and quasiparticle lifetime effect due to electron-phonon coupling was first experimentally identified on Mo(110) in 1999.[10]

The detailed characterization of the surface band structures near the Fermi level is particularly important in evaluating the effects of electron-phonon coupling in any material. Such an effect is most pronounced within the Debye energy $k_B\Theta_D$, which is several tens of milli-electron volts for transition metals. Electron-phonon coupling for the surfaces of molybdenum may provide insights into various kinds of surface structural phase transitions. In particular, the Mo(100) surface[12–19] is well known for the surface reconstructions, driven by Peierls-like instability[20–24] that results from the surface charge density wave transition due to the nesting of the Fermi surfaces. The Mo(112) surface, on the other hand, has a very anisotropic in-plane band structure[25–29] with strongly surface-weighted density of states. It is important to note that Mo(112) exhibits a significant surface relaxation, in which interlayer distances show large variations (e.g. >15% contraction for the first two layers from the surface) from the bulk-truncated value.[28,30,31]

The surface charge density of the Mo(112) substrate is a significant factor in the formation of well-ordered quasi-one-dimensional structures, such as seen for Li/Mo(112),[32,33] Sr/Mo(112),[34–37] Ba/Mo(112),[38] and Gd/Mo(112),[39] where overlayer systems have in common very large lateral distances between the adjacent atomic chains, favorable for the quasi-one-dimensionality.[40] Yet to understand the rich physics of these ordered quasi-one-dimensional overlayers, the details of the Mo(112) band structure must be understood and thus drives us to reexamine the band structure of Mo(112) in far greater detail than before.

II. EXPERIMENT

High-resolution angle-resolved photoemission spectroscopy (ARPES) was performed at the linear undulator beamline (BL-1)[41] of Hiroshima Synchrotron Radiation Center (HiSOR) at Hiroshima University, Japan. The surface of the Mo(112) sample was cleaned by the standard method of repeated annealing (at ∼1400 °C) in oxygen atmosphere with the oxygen partial pressure of $\sim 1 \times 10^{-6}$ torr, followed by cycles of annealing at 1000–1300 °C and flashing at ∼1800 °C, similar to the procedures used elsewhere.[25–28,42] Low-energy electron diffraction (LEED) and Auger electron spectroscopy (AES) were used to verify the quality of the Mo(112) surface, including the periodic structural order. The amount of surface contamination, such as C and O, were evaluated to be below the detection limit of the AES.

The high-resolution ARPES spectra were taken along the two high-symmetry lines ($\bar{\Gamma}-\bar{X}$ and $\bar{\Gamma}-\bar{Y}$ directions) of the surface Brillouin zone (SBZ), schematically illustrated in Fig. 1, with the *s*- and *p*-polarization geometries (with the electric field vector of the incident plane-polarized light parallel to the surface and within the plane containing the surface normal, respectively). The ARPES experiments were carried out using an angular (display) mode of the hemispheric electron analyzer (R4000, VG-Scienta) with the acceptance angle of $\pm 15^{\circ}$. The experimental band-structure mapping

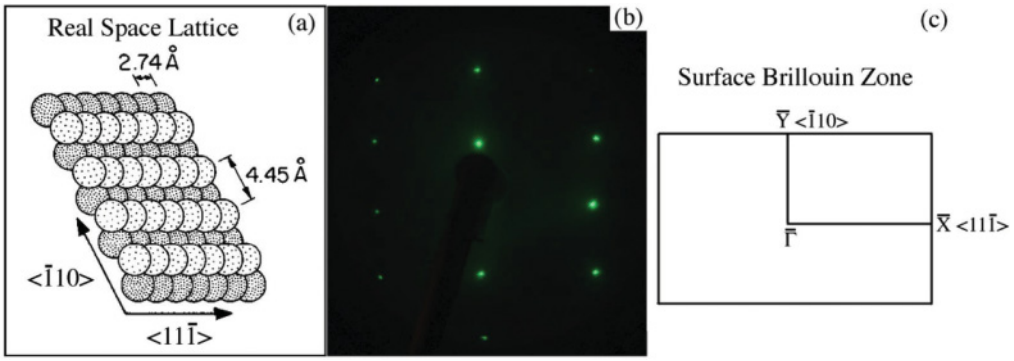

FIG. 1. (Color online) The atomic structure of Mo(112) in real and reciprocal space. (a) The schematic of real space structure. (b) The LEED pattern with $\langle\bar{1}10\rangle$ direction aligned vertically. (c) The surface Brillouin zone of Mo(112).

was performed using the incident photon energy of $\hbar\omega = 22$ eV. The combined energy resolution was estimated to be 10 meV, and the angular resolution was 0.3°, corresponding to the wave vector resolution of 0.01 ± 0.001 Å^{-1} at the Fermi level. The obtained ARPES spectra were not seen to be completely symmetric about $\bar{\Gamma}$ in the p-polarization geometry, which likely derives from the small misalignment of the sample. In addition, the electromagnetic field component perpendicular to the surface may vary due to the presence of a vacuum-solid interface, which may give rise to a nontrivial dependence of the photoemission matrix elements on photon incident angle[43–50] so that, in photoemission from surfaces for p-polarized geometry, there could be some apparent variation in the occupied band intensities measured as a function of wave vector. For this reason, we have taken the averaged experimental band mapping on both sides of $\bar{\Gamma}$. Thus, Figs. 2(b) and 2(e) represent the band structure along $\bar{\Gamma} - \bar{X}$ integrated over a finite thickness in k_y. The temperature of the sample was maintained at 50 K[51] throughout by a constant flow of liquid helium. Throughout the discussion, the binding energies are referenced to the Fermi energy (E_F), in terms of $E_F - E$.

III. THEORETICAL METHODOLOGY

The ARPES band mapping has been compared to DFT semirelativistic calculations in generalized gradient approximation (GGA)[52] performed with the ABINIT[53] package using Troullier–Martins norm-conserving pseudopotentials.[54] The periodicity in the direction normal to the surface was maintained by adopting the repeat-slab model. The slabs were built of 7 layers of Mo(112) atomic planes. The vacuum gap was about 10 Å. The optimizations of the atomic positions were performed until all forces became less than 0.05 eV/Å. The energy cutoff of 20 Hartrees (Ha) and 8 × 5 × 1 Monkhorst–Pack set of special k points provided the 0.001 Ha convergence of the total energy. The band structure along the high-symmetry lines in the SBZ was calculated with a small step (0.036 Å^{-1}, corresponding to 33 k points within the $\bar{\Gamma} - \bar{X}$ line), which was found to be important to reveal the details of surface resonance bands in vicinity of E_F.

Surface weights for every band and k point were estimated by integration of the partial local electron density within the atomic spheres (with $r = 2.5$ Bohr), using postprocessing tools of the ABINIT. As the next-to-surface atomic layer of the open Mo(112) surface can, in fact, also be attributed to the surface, the surface resonances correspond to the localization of the wave function within the first two surface layers. Some surface-derived states were found to be strongly localized to the top two surface layers (with weights of more than 90%), as discussed below. The symmetry of the surface bands was determined from the dominant partial weights of the states decomposed into spherical harmonics at the surface atoms.

Additional band-structure calculations based on 9- and 13-layer-thick slabs of Mo(112) were performed in order to minimize the possible misinterpretation of the computational artifacts of the of the 7-layer slab calculation. Although the 7-layer slab calculation should reproduce most of the essential features of the band structure derived from the surface, these additional calculations serve to distinguish the possible artificial surface resonances (i.e. arising solely due to the limited slab thickness) from the real surface resonances.

In order to further distinguish the surface ARPES spectral contribution from the pure bulk states, the bulk band structure projected onto the (112) surface was also calculated. In this calculation, the Mo unit cell was constructed such that the projected two-dimensional Brillouin zone matched the surface Brillouin zone (SBZ) of Mo(112). The projector augmented-wave (PAW)[55] Perdew–Burke–Ernzerhof (PBE)[52] pseudopotential within the density functional theory (DFT) band structure approach as implemented in VASP code[56,57] has been utilized. Mo 4p, 4d, and 5s are treated as valence orbitals in the pseudopotential. The kinetic energy cutoff of 340 eV and 8 × 12 × 4 Monkhorst–Pack[58] k points were taken for Brillouin zone sampling.

IV. THE BAND STRUCTURE ALONG THE TWO HIGH-SYMMETRY DIRECTIONS OF MO(112)

Utilization of linearly polarized light, as is available from synchrotron light sources, enables us to exploit the dipole selection rules for the photoemission process and allows us to clarify the symmetry properties of the electronic states in solids.[59–61] For the photoemission from the electronic states of Mo(112), the pertinent point group symmetry is C_{2v} at $\bar{\Gamma}$, $\bar{X}$, $\bar{Y}$, and C_{1h} along the two high-symmetry directions ($\bar{\Gamma} - \bar{X}$ and $\bar{\Gamma} - \bar{Y}$). Assuming that the final state of photoemission can be described by the plane-wave traveling to the photoelectron analyzer, the photoelectrons in the final state transform as the fully

TABLE I. The dipole selection rules for the electronic states at $\bar{\Gamma}$, $\bar{X}$, $\bar{Y}$ points (C_{2v}) and along the $\bar{\Gamma}-\bar{X}$ and the $\bar{\Gamma}-\bar{Y}$ directions (C_{1h}).

High symmetry points and lines[a]	Symmetry group	Irreducible representations (basis functions)[b]	Allowed initial symmetries[c]		
			A$\|x$	A$\|y$	A$\|z$
$\bar{\Gamma}-\bar{X}$	C_{1h}	A′ (x, z, z^2, xz, x^2-y^2)	A′	A″	A′
		A″ (y, xy, yz)			
$\bar{\Gamma}-\bar{Y}$	C_{1h}	A′ (x, z, z^2, xz, x^2-y^2)	A″	A′	A′
		A″ (y, xy, yz)			
$\bar{\Gamma}$, $\bar{X}$, $\bar{Y}$	C_{2v}	A_1 (z, z^2)	B_1	B_2	A_1
		A_2 (xy)			
		B_1 (x, xz)			
		B_2 (y, yz)			

[a]The x and y axes are defined parallel to $\bar{\Gamma}-\bar{X}$ and $\bar{\Gamma}-\bar{Y}$, respectively, and the z axis is along the surface normal direction.
[b]The irreducible representations in each point group are listed with the representative rectangular representations in parentheses.
[c]Allowed initial state symmetries in the photoemission are listed for each direction of incident light polarization determined by the vector potential A. For the ARPES taken along the $\bar{\Gamma}-\bar{X}$ direction, the vector potential in the s-polarized geometry only has a y component, and that of the p-polarized geometry has the mixture of x and z components. Similarly, for the ARPES taken along the $\bar{\Gamma}-\bar{Y}$ direction, the vector potential in the s-polarized geometry only has an x component, and that of the p-polarized geometry has the mixture of y and z components. The final state of photoemission is assumed to be described by a plane wave, which transforms as the fully symmetric representations, A_1 and A′, in both symmetry groups of C_{2v} and C_{1h}, respectively.

symmetric representation in both groups of C_{2v} and C_{1h}. Under these assumptions, we may identify the symmetries of the initial states allowed to make a photoemission transition.[59–61] These allowed initial symmetries are summarized in Table I according to the directions of light polarization. Note that, throughout the present discussion, the coordinate axes are defined so that the $\langle 11\bar{1}\rangle$ direction (the $\bar{\Gamma}-\bar{X}$ direction in SBZ) coincides with the x axis and the $\langle \bar{1}10\rangle$ direction (the $\bar{\Gamma}-\bar{Y}$ direction in SBZ) coincides with the y axis. Since the direction of light incidence and photoelectron detection lie within the same plane (xz plane for the spectra taken along the $\bar{\Gamma}-\bar{X}$ direction and yz plane for the spectra taken along the $\bar{\Gamma}-\bar{Y}$ direction), the vector potential of incident light in the p-polarization (s-polarization) geometry lies in the xz plane (y axis) for the spectra taken along the $\bar{\Gamma}-\bar{X}$ direction and lies in the yz plane (x axis) for the spectra taken along the $\bar{\Gamma}-\bar{Y}$ direction.

A. The band structure along the $\bar{\Gamma}-\bar{X}$ direction

While two bands have been observed to cross the Fermi level at 0.45 ± 0.05 and 0.59 ± 0.05 Å^{-1} along the $\bar{\Gamma}-\bar{X}$ direction in ARPES,[25,26,28] with the higher resolution and improved sensitivity of ARPES, three additional bands can now be observed and resolved crossing the Fermi level along the $\bar{\Gamma}-\bar{X}$ direction, as seen in the experimental band structure in Fig. 2. Figure 2(b) shows the ARPES band mapping taken along the $\bar{\Gamma}-\bar{X}$ direction with the p-polarized geometry. Four bands are found to cross the Fermi level (labeled as p_1, p_2, p_3, and p_4). The Fermi level crossings of the p_1 and p_2 bands are identified to be 0.47 and 0.60 Å^{-1}, respectively, and are consistent with the previously observed values.[25,26,28] The newly found bands, labeled as p_3 and p_4, are seen to cross the Fermi level at 0.64 and 0.81 Å^{-1}, respectively, as summarized in Table II. It is known that for the electronic states along the $\bar{\Gamma}-\bar{X}$ direction, the symmetry of the wave function can be classified either as even (A′ representation) or odd (A″ representation) with respect to the reflection about the xz plane. Since the incident light polarization lies within the xz plane for the p-polarized geometry, the selection rule

TABLE II. Band crossings at the Fermi level.

Band[a]	k_F (Å^{-1}) experiment	k_F (Å^{-1}) theory[b]	Surface weight[c] (%)
p_1	0.47 ± 0.01	0.48	51
p_2	0.60 ± 0.01	0.58	78
p_3	0.64 ± 0.01	0.65[d]	
p_4	0.81 ± 0.01	0.82	91
p_4	0.81 ± 0.01	0.88	90
s_1	0.22 ± 0.01	0.27	52
s_2	∼0.4 − 0.5	0.40 − 0.62	62 − 77
y_1	0.34 ± 0.01	0.36	81

[a]The band labels are defined in Figs. 2 and 3. The second and third columns compare the Fermi wave vector (k_F) for each band.
[b]The estimates of the wave vector of the Fermi level crossing in the 7-monolayer model, except for the p_3 band, which is compared to the bulk band-structure calculation.
[c]The estimates of the surface weight (the percentage charge localization within the first two layers in the 7-monolayer model) near the Fermi level are listed for each band, except for the p_3 band, which is a bulk band.
[d]Note that the experimentally observed p_3 band is not unambiguously reproduced in the 7-monolayer model calculation (see text). The Fermi level crossing for the p_3 band is compared to the bulk band-structure calculation

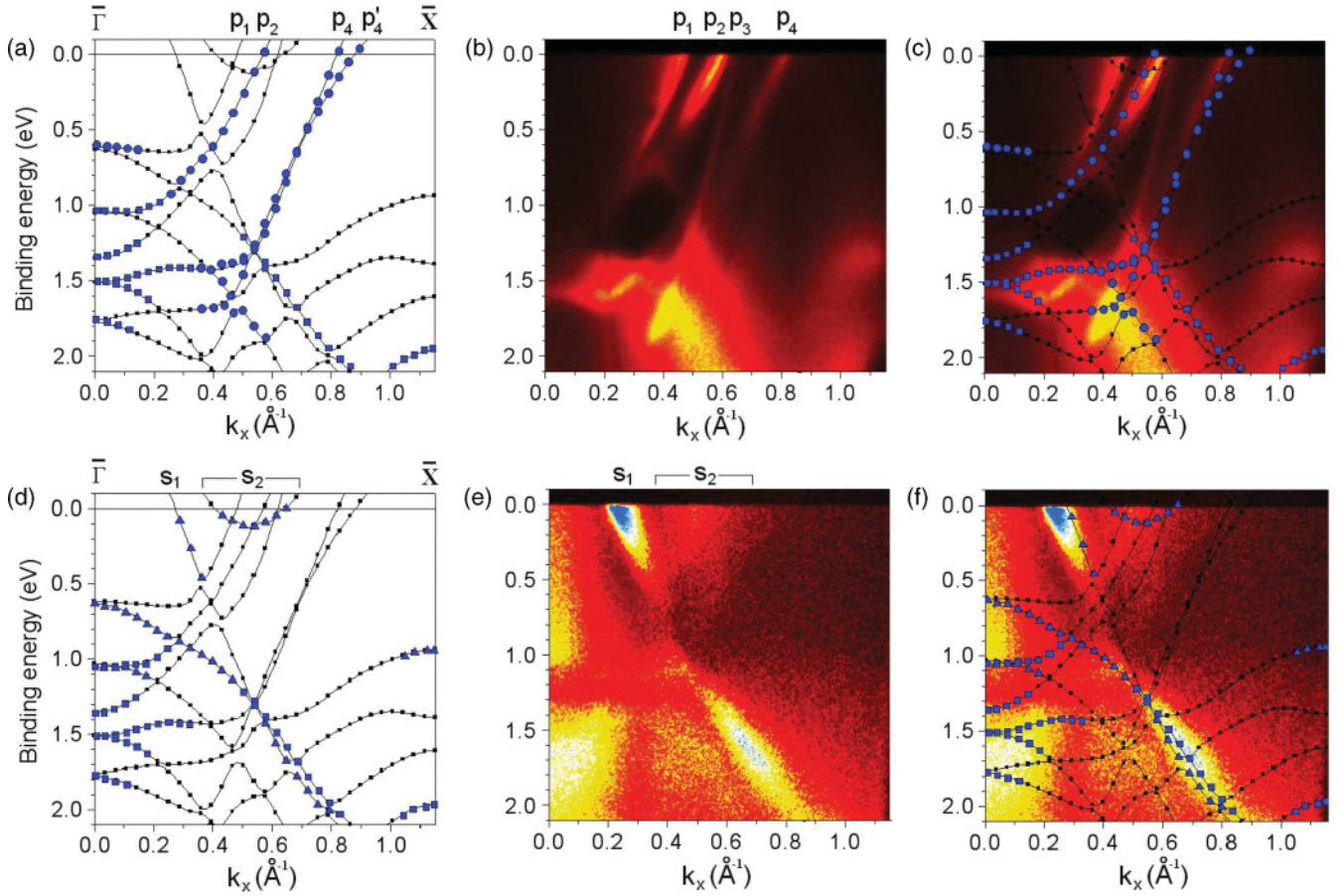

FIG. 2. (Color) The band structure of Mo(112) along the $\bar{\Gamma} - \bar{X}$ direction. (a) The calculated band structure with the 7-layer slab model. The states with noticeable surface weight (more than 60% charge localization within the first two layers) are marked with blue symbols (■,●) out of which circles (●) represent the states of clearly identified even symmetry with respect to the xz plane (A′ representation). (b) The ARPES band mapping taken with the p-polarized geometry at the photon energy of 22 eV. (c) The comparison of the calculated band structure with the ARPES band mapping taken with the p-polarized geometry. (d) The calculated band structure [same as (a)] but with the clearly identified odd states with respect to the xz plane (A″) marked with blue triangles (▲). (e) The ARPES band mapping taken with the s-polarized geometry at the photon energy of 22 eV. (f) The comparison of the calculated band structure with the ARPES band mapping taken with the s-polarized geometry.

(Table I) reveals that the light can only excite the electrons from the states with even reflection parity about the xz plane (A′). Thus, the four bands seen to cross the Fermi level in Fig. 2(b) are experimentally identified as even states for the binding energies near the Fermi level.

The results of the band-structure calculation based on the 7-layer slab model are shown in Fig. 2(a), and the calculated surface weights (defined here as the charge localization within the first two layers) near the Fermi level for selected bands are summarized in Table II. In Fig. 2(a), the states with noticeable surface weight are marked with blue symbols, and among those surface-weighted states, the clearly identified even states (A′) are marked with blue circles. The calculated band structure has been overlaid on the experimental ARPES band mapping, as shown in Fig. 2(c), and the respectable quantitative agreement is obtained between the theoretical and experimental band structures except for the p_3 band.

Among the four bands experimentally observed crossing the Fermi level along the $\bar{\Gamma} - \bar{X}$ direction, the band labeled p_1 was found to exhibit noticeable photon energy dependence. Although this band (p_1) is seen to cross the Fermi level at 0.47 Å^{-1} at the photon energy of 22 eV [Fig. 2(b)], the Fermi level crossing of this band is found to be 0.40 Å^{-1} at the photon energy of 50 eV and variously reported to be crossing the Fermi level with wave vectors as high as 0.54 Å^{-1}.[11,28] Such photon energy dependence indicates dispersion of the p_1 band along $k_\perp$ (the wave vector perpendicular to the surface) and suggests the bulk origin of the band. This identification is supported by the relatively small surface weight of 51% in the band-structure calculation, as summarized in Table II. Figure 3(b) shows the projected bulk band structure along the $\bar{\Gamma} - \bar{X}$ direction in which the calculated band structures at 10 different $k_\perp$ are overlaid. Since this calculation shows the high density of bulk bands that gives quantitative agreement with the p_1 band in ARPES band mapping, it serves to further confirm the bulk band structure origin of the p_1 band.

The p_2 band, with the Fermi level crossing at 0.60 Å^{-1} (experiment), was found to be sensitive to a small amount of surface contamination (the intensity of this band was seen to vary, while those of the other bands remained nearly constant).

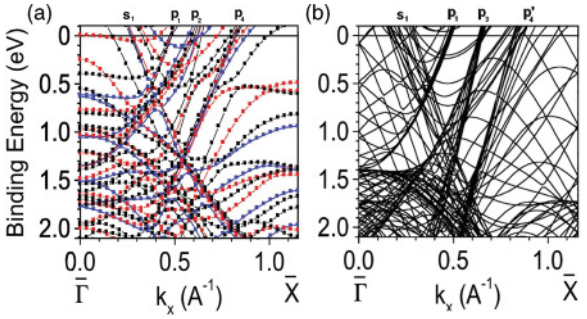

FIG. 3. (Color online) (a) The overlay of the calculated band structures along $\bar{\Gamma} - \bar{X}$ direction based on 7- (blue), 9- (red), and 13- (black) layer slab models, which is expected to show the surface-derived bands as well as some of the bulk bands. (b) The projected bulk band structure of Mo(112), which is composed of the band structures calculated along $\langle 11\bar{1} \rangle$ direction (i.e. parallel to $\bar{\Gamma} - \bar{X}$) at 10 different $k_\perp$. The bands identified in AREPS band mapping and calculated band structure based on 7-layer slab model (Fig. 2) are labeled correspondingly.

Such surface sensitivity of the p_2 band most likely derives from the fact that it carries a strong surface weight (78% as shown in Table II), and it can be seen in Fig. 2(c) that the calculated position of the band as well as its Fermi level crossing ($k_F = 0.58$ Å^{-1}) are in good agreement with the experiment. Since the projected bulk-band calculation, shown in Fig. 3(b), indicates no bulk band that exhibits the dispersion of the p_2 band in ARPES band mapping, evidently this band should not be identified as a bulk band. For these reasons, the p_2 band must largely be surface in origin and should be identified either as a surface resonance or true surface state of the Mo(112) surface. The further theoretical analysis revealed that the dominant orbital contributions to this band are of d_{z^2} and d_{xz} character, leading to the even reflection parity of the wave function near the Fermi level, which is consistent with the enhanced intensity of this band in the p-polarized spectrum and the diminished intensity in the s-polarized spectrum [Fig. 2(e)].

The p_3 band, with the Fermi level crossing at 0.64 Å^{-1} (experiment), is evident in the ARPES band mapping, but not reproduced in the band structure calculation based on the 7-layer slab model [Fig. 2(c)]. On the other hand, the calculated projected bulk band structure [Fig. 3(b)] clearly shows the presence of the densely spaced bulk bands in qualitative agreement with the p_3 band in observed in ARPES [Fig. 2(b)] in terms of both the position and the dispersion. Therefore, the band labeled p_3 (Fig. 2) likely originates from the bulk-band structure.

The p_4 band [Fig. 2(b)], with the Fermi level crossing at 0.81 Å^{-1} (experiment), was also found to exhibit surface sensitivity in the experiment. On the other hand, the result of the band-structure calculations based on 7-layer slab model suggest the existence of two closely spaced bands, labeled as p_4 and $p_4{}'$ in Fig. 2(a), with nearly equal significant surface weights (>90%) with the Fermi level crossings at 0.82 and 0.88 Å^{-1} (Table II). These two bands (p_4 and $p_4{}'$) both exhibit the predominant d_{z^2} orbital character (i.e. even states), hence the expected visibility in the experimental band structure taken in the p-polarized geometry. This apparent discrepancy that the closely spaced double bands are not observed in ARPES is resolved by comparing the calculations based on the slab models of different thickness. Figure 3(a) shows the overlay of the calculated band structures using 7-, 9-, and 13-layer slab models. In this comparison, it is seen that the p_4 band found in the 7-layer slab calculation remains nearly unchanged as the slab thickness is increased, which is evidence of surface localization of the p_4 band. However, the wave vector position of the $p_4{}'$ band is seen to be sensitive to the slab thickness, indicative of the greater bulk-band structure attributes of the $p_4{}'$ band. The calculated projected bulk band structure [Fig. 3(b)] further verifies this assignment. It is evident in this calculation that the bulk bands exhibiting the dispersion similar to $p_4{}'$ bands are present in the region of the p_4 and $p_4{}'$ bands. Thus, the comparison of the calculated band structures among the different slab thickness as well as the projected bulk band structure leads us to identify the $p_4{}'$ band in the 7-layer calculation [Fig. 2(a)] as the band from the bulk continuum that appears near the p_4 surface-derived band. Furthermore, since the surface-derived p_4 band lies within this bulk continuum, which shares the same symmetry with that of the p_4 band, this band is likely identified as surface resonance, not the true surface band.

Figure 2(e) shows the experimental ARPES band mapping taken along the $\bar{\Gamma} - \bar{X}$ direction with the s-polarized geometry. It is evident that the band structure acquired in the s-polarized geometry is significantly different from that taken with the p-polarized geometry. In Fig. 2(e), there is a distinct band (labeled as s_1) with downward dispersion (towards greater binding energy) away from $\bar{\Gamma}$. Note that the s_1 band loses most of its intensity between 0.5 and 1.2 eV. The results of the band-structure calculation are shown in Fig. 2(d), where the states with noticeable surface weight are marked with blue symbols and the electronic states clearly identified as odd (A″) with respect to the xz plane are marked with blue triangles. The position of the Fermi level crossing for this band (s_1) is in respectable agreement with the calculation for both clearly discernable parts (above 0.5 eV and below 1.2 eV) of this band, as seen in Fig. 2(f) and Table II. Since the incident light polarization lies along the y axis for the s-polarized geometry, by the selection rules (Table I), the symmetry of this electronic state is identified to be odd under the reflection about the xz plane (A″). The strong photoemission intensity of this downward-dispersing band in the experimental band structure in the s-polarized geometry is in agreement with our expectations from the calculation (odd states are signified with blue triangles). We suggest that the s_1 band originates mostly from the bulk state continuum above 0.5 eV, as the calculated projected bulk band structure also reproduces the bands with very similar dispersions and positions to those of the s_1 band, as shown in Fig. 3(b). On the other hand, the lower part (below 1.2 eV) of the s_1 band should contain noticeable surface weight as it is only reproduced in the surface slab calculations [Fig. 3(a)], but not in the bulk calculation.

The band structure calculations also predicts the existence of the shallow band crossing the Fermi level at 0.40 and 0.62 Å^{-1}, much like an electron pocket [labeled as s_2 in Fig. 2(d)]. This band is predicted to be of odd reflection parity (hence is expected to be visible only in the experimental band structure taken in the s-polarized geometry). The s_2 electron pocket is likely observed as the glowing region in

the experimental band structure obtained in the s-polarized geometry [Fig. 2(e)]. Although the 7-layer slab calculation indicates the discernable surface weight of this band (between 62% and 77% depending on the wave vector $k_{\parallel}$), we find in the comparison of 7-, 9-, and 13-layer slab calculations that the position of the band in wave vector k [but not its shape, that is to say the dispersion in $E(k)$] exhibits a noticeable dependence on the slab thickness, as seen in Fig. 3(a). Furthermore, the projected bulk band calculation [Fig. 3(b)] reproduced the bands of very similar characteristics (i.e. the electron-pocket-like bands between 0.4 and 0.7 Å^{-1} that shifts vertically as a function of $k_{\perp}$). Thus, it is likely that the band labeled s_2, identified in ARPES band mapping and the calculations based on the 7-layer slab [Fig. 2(d) and 2(e)], is part of the projection of a bulk band. It is worthwhile to note, at the same time, that the s_2 band is predicted to exhibit fairly steep dispersion along $k_{\perp}$, as can be seen from the large spacing among the s_2 projected bulk bands in Fig. 3(c). Such steep dispersion in $k_{\perp}$ direction may have caused the spread of ARPES intensity in the wide range, as seen Fig. 2(e).

B. The band structure along the $\bar{\Gamma} - \bar{\mathrm{Y}}$ direction

Due to the large in-plane interatomic distance along the $\langle \bar{1}10 \rangle$ direction (4.45 Å), the electronic band structure along the $\bar{\Gamma} - \bar{\mathrm{Y}}$ direction is expected to be much less dispersive than in the $\langle 11\bar{1} \rangle$ direction (the $\bar{\Gamma} - \bar{\mathrm{X}}$ direction). This general tendency is evident in the experimental as well as in the calculated band structures, as shown in Fig. 4. Along the $\bar{\Gamma} - \bar{\mathrm{Y}}$ direction, we note that the vector potential of incident light in the p-polarized geometry lies within the yz plane, and that of the s-polarized geometry lies along the x axis. This dictates the selection rule for the ARPES along the $\bar{\Gamma} - \bar{\mathrm{Y}}$ direction, as summarized in Table I.

Figure 4(b) shows the experimental band structure obtained along the $\bar{\Gamma} - \bar{\mathrm{Y}}$ direction with the p-polarized incident light geometry. The characteristic crossing of the bands (band folding) seen at $k_{\parallel} = 0.70$ Å^{-1} and binding energy $= 2.3$ eV (2.4 eV in calculated band structure) experimentally places the edge of the surface Brillouin zone ($\bar{\mathrm{Y}}$) and is consistent with the value determined from the surface structure (0.706 Å^{-1}). Of particular interest in the band structure along the $\bar{\Gamma} - \bar{\mathrm{Y}}$ direction is the distinct parabolic band centered at $\bar{\Gamma}$, crossing the Fermi level at 0.34 Å^{-1} (labeled as y_1). This band is only evident in the ARPES band mapping obtained in the p-polarized geometry, indicating that the y_1 band is of even symmetry with respect to the yz reflection (A′) away from $\bar{\Gamma}$ and is of A_1 or B_2 symmetry at $\bar{\Gamma}$ (see Table I). The calculated band structure, in Fig. 4(a) (where again bands with significant surface weight are marked by blue symbols, and even symmetry states are marked by blue circles), shows good general agreement with the experimental band structure as shown in Fig. 4(c). In particular, there is an excellent agreement for the y_1 band in terms of dispersion, the placement of the Fermi level crossing ($k_F = 0.36$ Å^{-1} in theory), as well as the reflection parity away from $\bar{\Gamma}$ [i.e. calculated to be even as signified by the circles in Fig. 4(a)]. Furthermore, the band structure calculation reveals the predominant d_{z^2} orbital character and the noticeable surface weight (81%) for the y_1 band near the Fermi level.

To further verify the surface or bulk origin and weight of the y_1 band, band-structure calculations based on different slab thickness as well as the projected bulk band structure calculations were performed and compared for the $\bar{\Gamma} - \bar{\mathrm{Y}}$ direction. Figure 5(a) shows the overlay of slab calculations based on 7-, 9-, and 13-layer models. The y_1 band exhibits noticeable dependence on the slab thickness in the calculated band structure in terms of position and dispersion, an indication of bulk weight. On the other hand, the projected bulk band calculation, shown in Fig. 5(b), is not in good quantitative agreement with the y_1 band observed in ARPES. The ARPES band mapping is not expected to give precise agreement with the bulk band structure mapped along the straight line in bulk Brillouin zone because the sampling depth of $k_{\perp}$ in ARPES varies with the wave vector parallel with the surface for photoemission as a single photon energy; but even with this consideration in mind, quantitative agreement between the ARPES and the calculated bulk band structure is absent, particularly near the Fermi level. Such a discrepancy between experiment and theory may have arisen from two artificial effects of bulk and slab calculations that (1) the bulk calculation does not take into account any mixing of the states with surface-derived states, and (2) the present slab calculation does not properly include the mixing of the surface states with the bulk continuum for any weak surface resonance that penetrates into bulk more than 13 layers. We tentatively suggest that the y_1 band be identified as weakly surface weighted, particularly near the Fermi level (i.e. where the agreement between the bulk/slab calculations and ARPES is relatively poor).

Figure 4(e) shows the ARPES band mapping taken along the $\bar{\Gamma} - \bar{\mathrm{Y}}$ direction with the s-polarized geometry. In this experimental band structure, there is no distinct band crossing the Fermi level. Although there is noticeable continuous swath of photoemission intensity, which resembles an hourglass shape between 0.3 and 0.4 Å^{-1} near the Fermi level, this is likely a contribution from the projected bulk bands, as is suggested by comparison with the bulk band structure calculation in Fig. 5(b). As seen in Figs. 4(d) and 4(f), the band structure obtained by ARPES and the calculated band structure are in general agreement. The upward-dispersing band and the downward-dispersing band that merge at $\bar{\mathrm{Y}}$ near 2.3 eV, in Fig. 3(f), are most likely derived largely from the projected bulk bands. These bands are reproduced in the calculated projected bulk band structure. Since these bulk bands are only distinct in the s-polarized spectrum, they are experimentally identified as of odd symmetry.

C. The electronic states near $\bar{\Gamma}$

There are a number of distinct states observed near $\bar{\Gamma}$. Since the pertinent point group symmetry at $\bar{\Gamma}$ is C_{2v}, the symmetry of the electronic states at this point can be classified into A_1, A_2, B_1, and B_2 representations, as opposed to the even (A′) and odd (A″) classifications along the $\bar{\Gamma} - \bar{\mathrm{X}}$ and the $\bar{\Gamma} - \bar{\mathrm{Y}}$ directions. The utilization of the photoemission selection rules (Table I) allows us to clarify the symmetry properties of the electronic states at $\bar{\Gamma}$. Figure 6 shows the energy distribution curves (EDCs) of the photoemission spectra at $\bar{\Gamma}$ (integrated over ± 0.01 Å^{-1}) for the four distinct incident light polarizations (the polarization of vector potential

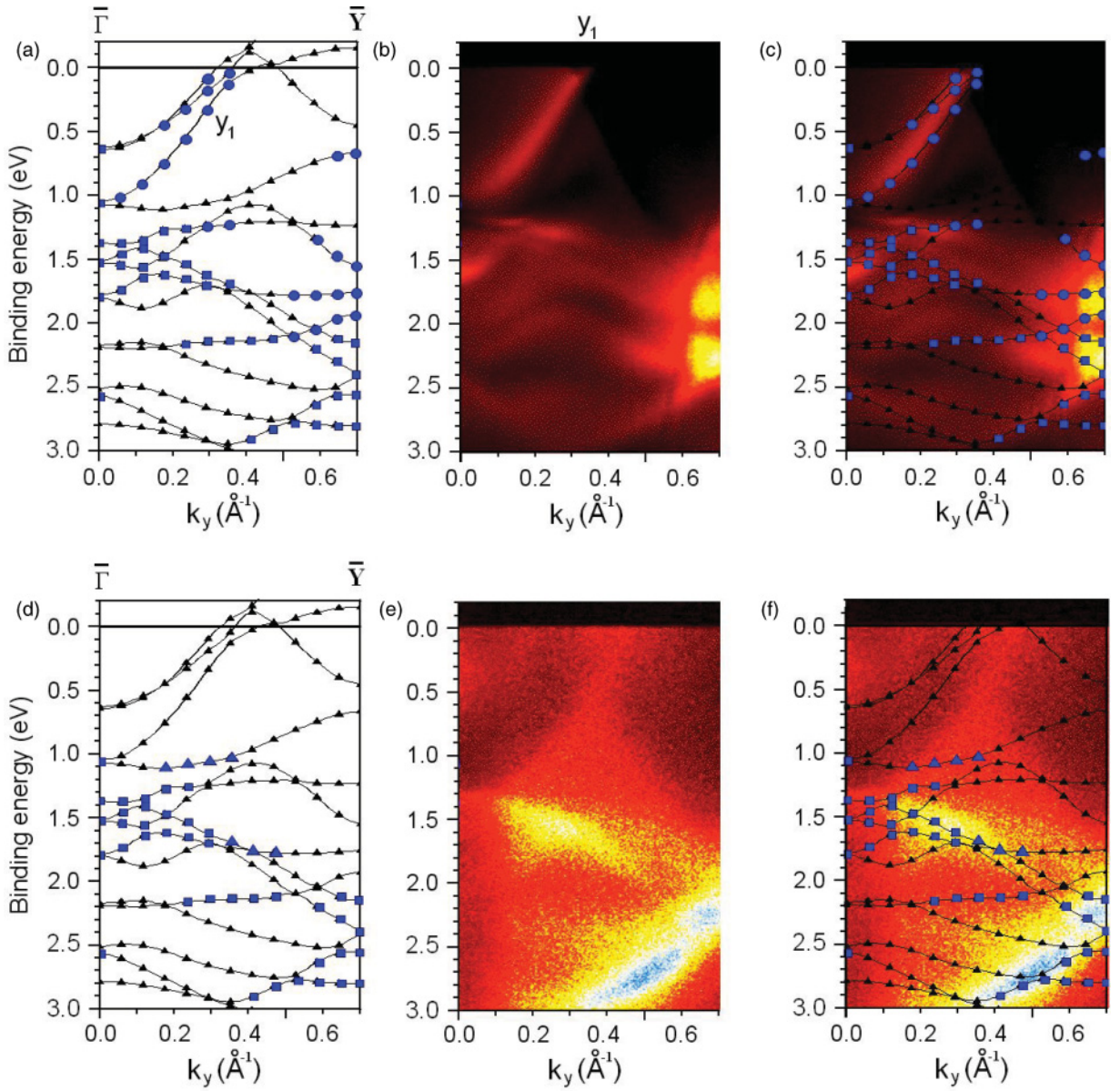

FIG. 4. (Color) The band structure of Mo(112) along the $\bar{\Gamma} - \bar{Y}$ direction. (a) The calculated band structure with the 7-layer slab model. The states with noticeable surface weight (more than 60% charge localization within the first two layers) are marked with blue symbols (■,●) out of which circles (●) represent the states of clearly identified even symmetry with respect to the yz plane (A′ representation). (b) The ARPES band mapping taken with the p-polarized geometry at the photon energy of 22 eV. (c) The comparison of the calculated band structure with the ARPES band mapping taken with the p-polarized geometry. (d) The calculated band structure [same as (a)] but with the clearly identified odd states with respect to the yz plane (A″) marked with blue triangles (▲). (e) The ARPES band mapping taken with the s-polarized geometry at the photon energy of 22 eV. (f) The comparison of the calculated band structure with the ARPES band mapping taken with the s-polarized geometry.

A for each EDC is noted in the legend). The peak at around the binding energy of 1.0 eV is identified in the spectra (b) and (c) in which the light polarization lies within the yz plane and along the y axis, respectively. The absence of this peak in the other two spectra is consistent and thus indicates that this state, at 1.0 eV binding energy near $\bar{\Gamma}$, is of B_2 symmetry. It was previously reported that the position of this band exhibited noticeable periodic photon energy dependence in the range of 18–83 eV.[25,26] Since our band structure calculations show the relatively low surface weight of 56–67% (note that the surface weight of this band near the Fermi level is estimated to be 81% along $\bar{\Gamma} - \bar{Y}$), this band at 1.0 eV binding energy near $\bar{\Gamma}$ is identified either as a projected bulk state or a surface resonance that is strongly hybridized with the bulk bands.

There is another peak at 1.5 eV binding energy near $\bar{\Gamma}$, which is pronounced only in the spectra (a) and (b) of Fig. 6. From the selection rules, this state is most likely of A_1 symmetry character. In fact, this is consistent with the previously suggested symmetry of this state as inferred from

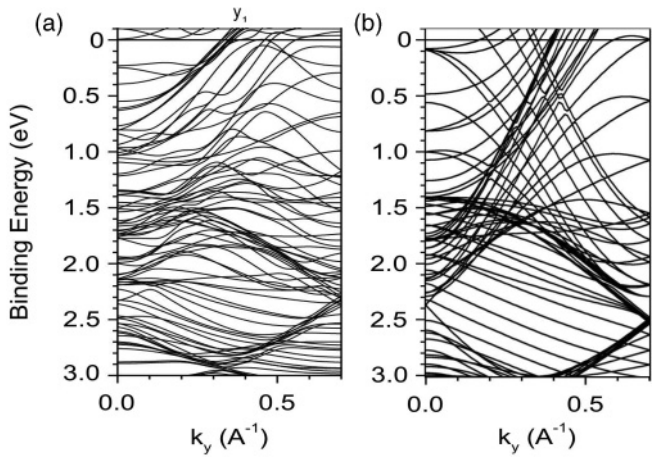

FIG. 5. (a) The overlay of the calculated band structures along $\bar{\Gamma} - \bar{Y}$ direction based on 7-, 9-, and 13-layer slab models, which is expected to show the surface-derived bands as well as some of the bulk bands. (b) The projected bulk band structure of Mo(112), which is composed of the band structures calculated along $\langle \bar{1}10 \rangle$ direction (i.e. parallel to $\bar{\Gamma} - \bar{Y}$) at 10 different $k_\perp$. The bands identified in AREPS band mapping and calculated band structure based on 7-layer slab model (Fig. 4) are labeled correspondingly.

the angular dependence of the photoemission intensity in the earlier study.[26] It was also reported that this state exhibited only weak, but discernable, photon energy dependence.[26] In fact our calculation identifies the significant surface charge localization for this state (87–92%), and thus we suggest attributing the

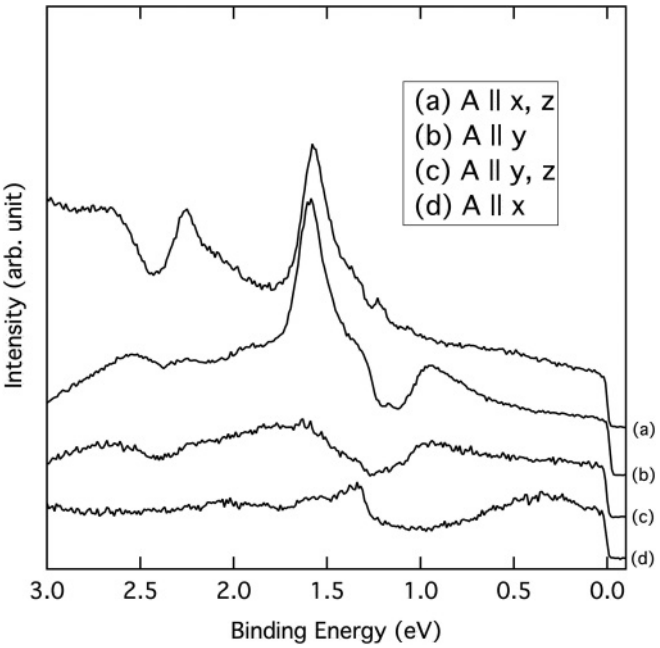

FIG. 6. The energy distribution curves (photoemission intensity vs binding energy) at $\bar{\Gamma}$ for the four different incident light polarization geometry. The data are obtained by integrating the ARPES spectra in Figs. 2(b) and 2(e) and Figs. 3(b) and 3(e) over ± 0.01 Å^{-1}. The nonvanishing component(s) of vector potential **A** for the four incident light polarization geometries are (a) x and z component, (b) y component, (c) y and z component, and (d) x component.

observed state, at a binding energy of 1.5 eV, to a surface resonance state.

It is important to point out that the symmetry identification of the band at the binding energy of 1.0 eV at $\bar{\Gamma}$ (B_2) requires that, while the p_2 band along $\bar{\Gamma} - \bar{X}$ [Figs. 2(a) and 2(b)[and the y_1 band along $\bar{\Gamma} - \bar{Y}$ [Figs. 4(a) and 4(b)] both reach $\bar{\Gamma}$ at around 1.0 eV binding energy, these two bands should not actually meet (or become degenerate) at $\bar{\Gamma}$, unless there is an accidental degeneracy. The reflection parity of a B_1 state is odd with respect to the xz plane, but even with respect to the yz plane. However, since the reflection parity of the p_2 band is identified as even with respect to the xz plane, the symmetry of the p_2 band is incompatible with the state found at 1.0 eV binding energy. Thus, the state of B_2 symmetry found at $\bar{\Gamma}$, in Fig. 6, must be attributed to the y_1 band but not to the p_2 band. Therefore, the vanishingly small ARPES intensity of the p_2 band near $\bar{\Gamma}$ cannot *a priori* be associated with photoemission selection rules.

V. COMPLICATIONS TO THE EXTRACTION OF ELECTRON-PHONON COUPLING FROM THE BAND STRUCTURE OF MO(112)

It was recently reported that there was a surface-weighted band along the $\bar{\Gamma} - \bar{X}$ direction on Mo(112), which exhibits an anomalously large distortion near the Fermi level in ARPES band mapping utilizing largely p-polarized synchrotron light source (photon energy = 18 eV).[28] Such distortion of the band was believed to originate solely from the band renormalization due to electron-phonon coupling on the surface. In a subsequent study,[11] the Fermi level crossing of this band was estimated to be about 0.54 Å^{-1}, and due to the previously reported presence of the surface-sensitive band at around 0.59 Å^{-1} (Refs. 25 and 26) [which we now identify as the p_2 band as in Figs. 2(a) and 2(b)], this band was mistakenly identified as the surface-weighted band. The present study, which reveals the details of band structure over the entire surface Brillouin zone (SBZ) along the $\bar{\Gamma} - \bar{X}$ direction, identifies this band (described in Ref. 11) as the largely bulk-derived p_1 band [Figs. 2(a) and 2(b)]. Therefore, the characterization of this band[11,28] as surface weighted is false, as it does not conserve two-dimensionality of state and retains significant photon energy dependence. We now believe that the observed band with anomalously large distortion near the Fermi level[11,28] is more correctly identified as containing significant bulk weight. Therefore, the electron-phonon coupling parameters extracted from this band should be attributed mostly to the bulk Mo rather than Mo(112) surface.

The detailed analysis[11] of the apparent renormalization of this bulk-weighted band (believed to be surface weighted at the time), with the Fermi level crossing in the region of 0.48 ± 0.08 Å^{-1}, provided the mutually consistent real and imaginary parts of self energy (i.e. they are related by the Kramers–Kronig relation). Some of the quantitative features of this apparent mass enhancement in the band structure near the Fermi level, however, are inconsistent with the recent theoretical calculation of the electron-phonon coupling for the bulk Mo.[62] The most evident discrepancy is in the Debye temperature (Θ_D) of Mo. Both calculations[62,63] and experiments[28,64] give the estimates Θ_D = 33–35 meV, but

the detailed analysis of the mass enhancement of surface resonance band with the Fermi level crossing at 0.54 $Å^{-1}$ yielded $\Theta_D \sim 60$ meV. Considering the strength of Eliashberg function of Mo[62] and the temperature of the sample (now estimated to be about 170 K), the observed distortion is anomalously large compared to the expectations for the binding energy above 10 meV.

With much better understanding of details of the Mo(112) band structure, it is now clear that there is a shallow band that likely originates from bulk continuum [marked as s_2 in Figs. 2(d) and 2(e)], much like an electron pocket, that crosses the p_1 band in the vicinity of the Fermi level along the $\bar{\Gamma} - \bar{X}$ direction. Since the observed electron pocket (s_2) is of odd symmetry, it remains largely absent in the ARPES band mapping taken with p-polarized light [Fig. 2(b)]. Although in principle, the p_1 band and s_2 electron pocket are not expected to hybridize due to the symmetry restrictions, the small imperfections in the linear polarization of light source could lead to a contribution of the odd-symmetry s_2 electron pocket to the spectral weight of the p_1 band observed in p-polarized light. In addition, the spin-orbit coupling on Mo(112) surface may give rise to the relaxation of the dipole selection rule (i.e. relativistic effects for the selection rule must be considered), since such corrections are known for metals of lower atomic number than Mo (e.g. Cu).[65–69] This small leakage of ARPES intensity from the odd-symmetry band into the p-polarized spectrum could be problematic when an accurate extraction of position and width of this band in the vicinity of the Fermi level is required, as is the case for the determination of electron-phonon coupling parameters.

The presence of the bulk band structure electron pocket near the Fermi level should create difficulties for extraction of electron-phonon coupling, especially if the spectral interference is not uniform in the region of the p_1 band close to the Fermi level (binding energy <100 meV and $k \approx 0.47$ $Å^{-1}$). This is the case in the present ARPES study with a photon energy of 22 eV. We believe such nonuniform spectral contributions of the s_2 electron pocket to the p_1 band in the recent experiment[11] could partly account for the observation of anomalously large distortion of the p_1 band and the apparently unusual electron-phonon coupling parameters. It is important to consider the possibility of spectral interference that may obscure accurate extraction of some of the parameters (e.g. Debye temperature) relevant to the electron-phonon coupling on Mo.

We must pay extra attention to the possible interaction between the bands as well as the possibility of multiple spectral contributions to the experimental band mapping before drawing any conclusion on the electron-phonon coupling parameters of this band. Thus, the complexity of the band structure of Mo(112) may impose potential difficulties in the experimental characterization of electron-phonon coupling on this surface, yet with a complete identification of the surface- and bulk-derived bands, there is now hope for a measurement condition better suited for experimental characterization of the electron-phonon coupling parameters.

In order to extract the electron-phonon coupling parameters for Mo(112) surface, it is critical to carefully investigate the surface-weighted band(s) in the close vicinity of the Fermi level (>100 meV). Using the present band identification, there are strongly surface-weighted bands that include the p_2 and p_4 bands along $\bar{\Gamma} - \bar{X}$ direction and the y_1 band along $\bar{\Gamma} - \bar{Y}$ direction. For the p_2 band, any investigation of electron-phonon coupling and resulting band renormalization investigation must be done carefully, as the s_2 electron pocket may obscure the band features pertinent to the electron-phonon coupling. Utilizing different photon energies in photoemission probes the bulk band structure at different depths in $k_\perp$. So a possible strategy to minimize such interference from the projected bulk band structure is to choose an appropriate photon energy for which the bulk electron pockets does not yield noticeable nonuniform intensity near the Fermi level and where the photoemission exhibits higher surface sensitivity (say some photon energies greater than 22 eV), but above all characterize bands which are unlikely to hybridize with the bulk band structure. The p_4 band crosses the Fermi level with significant surface weight and is not complicated by contributions from close or overlapping bands, at least in the present ARPES band mapping (the projected bulk states seem to contribute to relatively uniform background intensity), and the extraction of the electron-phonon coupling parameters may be more easily realized. The y_1 band (tentatively identified as surface resonance band) seen along the $\bar{\Gamma} - \bar{Y}$ direction is also predicted to lie close to other bands near the Fermi level according to the present calculation [Fig. 4(a)].

VI. SUMMARY

The band structures along the two high-symmetry directions, $\bar{\Gamma} - \bar{X}$ and $\bar{\Gamma} - \bar{Y}$, are shown to be significantly different, which is expected and serves to verify the strong anisotropy of the surface of Mo(112). By utilizing the light-polarization dependence of ARPES spectra and the dipole selection rules, the symmetry character of some bands are identified and seen to be in good agreement with the expectations. Our study suggests the existence of at least two surface resonance bands along the $\bar{\Gamma} - \bar{X}$ direction (with $k_F = 0.59$ and 0.81 $Å^{-1}$) and one along the $\bar{\Gamma} - \bar{Y}$ direction (with $k_F = 0.34$ $Å^{-1}$). Although investigations of the surface-weighted bands are critical in determining the detailed picture of electron-phonon coupling on Mo(112) surface, the complexity of the surface and projected bulk band structures of Mo(112) implies a number of possible experimental difficulties arising from the interferences of spectral distributions of closely located bands not previously recognized. We believe that the present band structure characterization of Mo(112) serves to better guide the future investigations on electron-phonon coupling as well as other many-body interactions of this surface.

ACKNOWLEDGMENTS

This work was partially supported by the IMI Program of the National Science Foundation under Award No. DMR 0843934 and the UNL NSF "QSPINS" MRSEC (DMR-0820521). The authors acknowledge the technical assistance of Koji Miyamoto at the Hiroshima Synchrotron Radiation Center (HiSOR). The experiments have been done under the approval of HiSOR (Proposal No. 10-B-32).

*Corresponding author: pdowben@unl.edu

[1] I. E. Tamm, Phys. Z. Soviet Union **1**, 732 (1932).
[2] A. W. Maue, Z. Phys. **94**, 717 (1935).
[3] W. Shockley, Phys. Rev. **56**, 317 (1939).
[4] E. T. Goodwin, Proc. Cambridge Philos. Soc. **35**, 205 (1939).
[5] E. T. Goodwin, Proc. Cambridge Philos. Soc. **35**, 221 (1939).
[6] E. T. Goodwin, Proc. Cambridge Philos. Soc. **35**, 232 (1939).
[7] S. Weng, Phys. Rev. Lett. **38**, 434 (1977).
[8] S. L. Weng, T. Gustafsson, and E. W. Plummer, Phys. Rev. Lett. **39**, 822 (1977).
[9] S. L. Weng, E. W. Plummer, and T. Gustafsson, Phys. Rev. B **18**, 1718 (1978).
[10] T. Valla, A. V. Fedorov, P. D. Johnson, and S. L. Hulbert, Phys. Rev. Lett. **83**, 2085 (1999).
[11] N. Wu, Ya. B. Losovyj, K. Fukutani, and P. A. Dowben, J. Phys.: Condens. Matter **22**, 245501 (2010).
[12] T. E. Felter, R. A. Barker, and P. J. Estrup, Phys. Rev. Lett. **38**, 1138 (1977).
[13] J. W. Chung, K. S. Shin, D. H. Baek, C. Y. Kim, H. W. Kim, S. K. Lee, C. Y. Park, S. C. Hong, T. Kinoshita, M. Watanabe, A. Kakizaki, and T. Ishii, Phys. Rev. Lett. **69**, 2228 (1992).
[14] K. E. Smith and S. D. Kevan, Phys. Rev. B **43**, 3986 (1991).
[15] X. W. Wang, C. T. Chan, K. M. Ho, and W. Weber, Phys. Rev. Lett. **60**, 2066 (1988).
[16] I. Terakura, K. Terakura, and N. Hamada, Surf. Sci. **103**, 103 (1981).
[17] E. Hulpke and D. M. Smilgies, Phys. Rev. B **40**, 1338 (1989).
[18] J. E. Inglesfield, J. Phys. C **11**, L69 (1978).
[19] J. E. Inglesfield, J. Phys. C **12**, 149 (1979).
[20] R. A. Barker, P. J. Estrup, F. Jona, and P. M. Marcus, Solid State Commun. **25**, 375 (1978).
[21] R. E. Peierls, *Quantum Theory of Solids* (Oxford University Press, Oxford, 1955).
[22] E. Tosatti, Solid State Commun. **25**, 637 (1978).
[23] H. Krakauer, M. Posternak, and A. J. Freeman, Phys. Rev. Lett. **43**, 1885 (1979).
[24] J. C. Campuzano, D. A. King, C. Somerton, and J. E. Inglesfield, Phys. Rev. Lett. **45**, 1649 (1980).
[25] T. McAvoy, J. Zhang, C. Waldfried, D. N. McIlroy, P. A. Dowben, O. Zeybek, T. Bertrams, and S. D. Barrett, Eur. Phys. J. B **14**, 747 (2000).
[26] I. N. Yakovkin, J. Zhang, and P. A. Dowben, Phys. Rev. B **63**, 115408 (2001).
[27] H. K. Jeong, T. Komesu, I. N. Yakovkin, and P. A. Dowben, Surf. Sci. Lett. **494**, L773 (2001).
[28] N. Wu, Ya. B. Losovyj, Z. Yu, R. F. Sabirianov, W. N. Mei, N. Lozova, J. A. Colón Santana, and P. A. Dowben, J. Phys.: Condens. Matter **21**, 474222 (2009).
[29] I. N. Yakovkin, Surf. Sci. **389**, 48 (1997).
[30] I. N. Yakovkin, Eur. Phys. J. B **44**, 551 (2005).
[31] D. Kolthoff, H. Pfnür, A. G. Fedorus, V. Koval, and A. G. Naumovets, Surf. Sci. **439**, 224 (1999).
[32] A. Fedorus, D. Kolthoff, V. Koval, I. Lyuksyutov, A. G. Naumovets, and H. Pfnur, Phys. Rev. B **62**, 2852 (2000).
[33] A. Kiejna and R. M. Nieminen, Phys Rev. B **66**, 085407 (2002).
[34] A. Fedorus, G. Godzik, V. Koval, A. Naumovets, and H. Pfnur, Surf. Sci. **460**, 229 (2000).
[35] A. Kiejna and R. M. Nieminen, Phys. Rev. B **69**, 235424 (2004).
[36] V. K. Medvedev and I. N. Yakovkin, Fiz. Tverd. Tela **20**, 928 (1978).
[37] V. K. Medvedev and I. N. Yakovkin, Fiz. Tverd. Tela **21**, 313 (1979); Sov. Phys. Solid State **21**, 187 (1979).
[38] V. K. Medvedev and I. N. Yakovkin, Fiz. Tverd. Tela **23**, 669 (1981).
[39] Ya. B. Losovyj, I. N. Yakovkin, H. K. Jeong, D. Wisbey, and P. A. Dowben, J. Phys.: Condens. Matter **16**, 4711 (2004).
[40] I. N. Yakovkin, J. Nanosci. Nanotechnol. **1**, 357 (2001).
[41] K. Shimada, M. Arita, Y. Takeda, H. Fujino, K. Kobayashi, T. Narimura, H. Namatame, and M. Taniguchi, Surf. Rev. Lett. **9**, 529 (2002).
[42] K. Fukutani, Ya. B. Losovyj, N. Lozova, N. Wu, and P. A. Dowben, J. Electron Spectrosc. Relat. Phenom. **184**, 318 (2011).
[43] P. J. Feibelman, Phys. Rev. B **12**, 1319 (1975).
[44] H. J. Levinson, E. W. Plummer, and P. J. Feibelman, Phys. Rev. Lett. **43**, 952 (1979).
[45] T. Miller, W. E. McMahon, and T. C. Chiang, Phys. Rev. Lett. **77**, 1167 (1996).
[46] E. D. Hansen, T. Miller, and T. C. Chiang, Phys. Rev. Lett. **78**, 2807 (1997).
[47] T. Miller, E. D. Hansen, W. E. McMahon, and T. C. Chiang, Surf. Sci. **376**, 32 (1997).
[48] F. Pforte, T. Michalke, A. Gerlach, A. Goldmann, and R. Matzdorf, Phys. Rev. B **63**, 115405 (2001).
[49] V. B. Zabolotnyy, S. V. Borisenko, A. A. Kordyuk, D. S. Inosov, A. Koitzsch, J. Geck, J. Fink, M. Knupfer, B. Buchner, S. L. Drechsler, V. Hinkov, B. Keimer, and L. Patthey, Phys. Rev. B **76**, 024502 (2007).
[50] N. J. Speer, M. K. Brinkley, Y. Liu, C. M. Wei, T. Miller, and T. C. Chiang, EuroPhys. Lett. **88**, 67004 (2009).
[51] Temperature is confirmed by deconvolution of the experimental width of the Fermi function and the expected instrumental broadening.
[52] J. P. Perdew, K. Burke, and M. Ernzerhof, Phys. Rev. Lett. **77**, 3865 (1996).
[53] X. Gonze, J. M. Beuken, R. Caracas, F. Detraux, M. Fuchs, G. M. Rignanese, L. Sindic, M. Verstraete, G. Zerah, F. Jollet, M. Torrent, A. Roy, M. Mikami, Ph. Ghosez, J. Y. Raty, and D. C. Allan, Comput. Mater. Sci. **25**, 478 (2002).
[54] N. Troullier and J. L. Martins, Phys. Rev. B **43**, 1993 (1991).
[55] P. E. Blöchl, Phys. Rev. B **50**, 17953 (1994).
[56] G. Kresse and J. Furthmüller, Comput. Mater. Sci. **6**, 15 (1996).
[57] J. Paier, R. Hirschl, M. Marsman, and G. Kresse, J. Chem. Phys. **122**, 234102 (2005).
[58] H. Monkhorst and J. Pack, Phys. Rev. B **13**, 5188 (1976).
[59] P. A. Dowben, J. Choi, E. Morikawa, and B. Xu, in *Handbook of Thin Films*, edited by H. S. Nalwa, (Academic Press, San Diego, CA, 2002) Ch. 2, Vol. 2, pp. 61–114.
[60] J. Hermanson, Solid State Commun. **22**, 9 (1977).
[61] W. Eberhardt and F. J. Himpsel, Phys. Rev. B **21**, 5572 (1980).
[62] I. N. Yakovkin and P. A. Dowben, J. Phys.: Condens. Matter **23**, 225503 (2011).
[63] S. Y. Savrasov and D. Y. Savrasov, Phys. Rev. B **54**, 16487 (1996).
[64] C. Waldfried, D. N. McIlroy, J. Zhang, P. A. Dowben, G. A. Katrich, and E. W. Plummer, Surf. Sci. **363**, 296 (1996).
[65] H. Przybylski, A. Baalmann, G. Borstel, and M. Neumann, Phys. Rev. B **27**, 6669 (1983).
[66] S. C. Wu, H. Li, Y. S. Li, D. Tian, and F. Jona, Phys. Rev. B **44**, 13308 (1991).
[67] G. Borstel, M. Neumann, and M. Wohlecke, Phys. Rev. B **23**, 3121 (1981).
[68] G. Borstel, H. Przybylski, M. Neumann, and M. Wohlecke, Phys. Rev. B **25**, 2006 (1982).
[69] R. J. Elliott, Phys. Rev. **96**, 280 (1982).